Carbon nanofiber growth in plasma-enhanced chemical vapor deposition

I. Denysenko, K. Ostrikov, U. Cvelbar, M. Mozetic, and N. A. Azarenkov

---

Carbon nanofiber growth in plasma-enhanced chemical vapor deposition

I. Denysenko,[1,2,a)] K. Ostrikov,[3,1,4] U. Cvelbar,[4] M. Mozetic,[4] and N. A. Azarenkov[2]

[1]*Plasma Nanoscience, School of Physics, The University of Sydney, Sydney, New South Wales 2006, Australia*
[2]*School of Physics and Technology, V. N. Karazin Kharkiv National University, 4 Svobody sq., 61077 Kharkiv, Ukraine*
[3]*CSIRO Materials Science and Engineering, Lindfield, New South Wales 2070, Australia*
[4]*Jozef Stefan Institute, Jamova cesta 39, Ljubljana SI 1000, Slovenia*

A theoretical model to describe the plasma-assisted growth of carbon nanofibers (CNFs) is proposed. Using the model, the plasma-related effects on the nanofiber growth parameters, such as the growth rate due to surface and bulk diffusion, the effective carbon flux to the catalyst surface, the characteristic residence time and diffusion length of carbon atoms on the catalyst surface, and the surface coverages, have been studied. The dependence of these parameters on the catalyst surface temperature and ion and etching gas fluxes to the catalyst surface is quantified. The optimum conditions under which a low-temperature plasma environment can benefit the CNF growth are formulated. These results are in good agreement with the available experimental data on CNF growth and can be used for optimizing synthesis of related nanoassemblies in low-temperature plasma-assisted nanofabrication. © *2008 American Institute of Physics*. [DOI: 10.1063/1.2986915]

I. INTRODUCTION

Recently, there has been a significant interest in high-aspect-ratio nanostructures (e.g., nanotubes, nanofibers, nanoribbons, nanorods, and nanowires) due to their many potential applications such as atomic force microscope tips, superhydrophobic surfaces, field emitter devices, synthetic membranes, intracellular gene delivery devices, biosensors, and several others.[1–12] These nanostructures may also be useful in production of high strength composites, interconnects and field-effect transistors, in electron beam lithography, and for storage of hydrogen, lithium, and other metals.[13,14]

Various high-aspect-ratio nanostructures have been synthesized by different methods including laser vaporization, arc discharge, thermal chemical vapor deposition (CVD), and plasma-enhanced CVD (PECVD).[1,2,15–20] In particular, PECVD techniques have been successfully used for the production of well-aligned carbon nanotubes (CNTs) and carbon nanofibers (CNFs). Experiments have shown that carbon nanostructures may be grown via PECVD at significantly lower substrate temperatures and feature better alignment compared to nanostructures synthesized in thermal processes.[2,21]

However, in order to control the growth of CNFs and CNTs one has to properly understand and be able to effectively manage the plasma properties as well as numerous elementary processes on the substrate. Several properties of low-temperature plasmas used for the growth of CNFs and other carbon nanostructures have been investigated theoretically and experimentally by many authors.[1,8,22–25] Meanwhile, processes on the catalyst that accompany the CNF and CNT formation have received little attention compared to similar processes in CVD (Refs. 26 and 27) and are still very far from being properly understood.

In a letter article[28] we reported on the growth kinetics of CNFs in a hydrocarbon plasma. In particular, it was shown that at low temperatures the nanofibers grow via surface diffusion of carbon atoms[29] produced on a catalyst particle via ion-induced dissociation of a hydrocarbon precursor.[28] Effects of ion and etching gas fluxes on the growth of single walled CNTs were studied by Denysenko *et al.*[30]

The present paper extends the scope of the letter article[28] and provides additional in-depth study and interpretation of the processes on the surface of the catalyst particles that accompany the catalytic CNF growth. In particular, we investigate how ion and etching gas fluxes from a hydrocarbon plasma affect the surface coverage of the catalyst surface by different species, the effective carbon flux to the catalyst, the characteristic residence time, and the surface diffusion length of carbon adatoms on the catalyst surface. We also analyze how the growth parameters depend on the catalyst surface temperature and hydrogen adsorption and compare the dependencies obtained in the plasma-assisted and thermal CVD processes. Our results are applied to the available experimental data on CNF and CNT growth in PECVD.[9,21,31,32]

The structure of this paper is as follows. Section II presents the main assumptions of the CNF growth model, in addition to the complete set of model equations used. In Sec. III, the analytical solutions for the surface coverages and diffusion fluxes of carbon atoms to the graphene sheets of the CNFs are presented. Section IV is devoted to the study of the growth parameters as functions of the catalyst surface temperature and the ion and etching gas densities. In Sec. V, we discuss the plasma-related effects on the CNF growth, as well as some important assumptions used in the CNF growth model. Conclusions and outlook for the future research are given in Sec. VI.

II. BASIC ASSUMPTIONS AND MAIN EQUATIONS

In this section we present basic assumptions and main equations of the plasma-assisted growth of a CNF with a metal catalyst particle on its top. It is assumed that the top

---

a)Author to whom correspondence should be addressed. Electronic mail: deny@physics.usyd.edu.au.
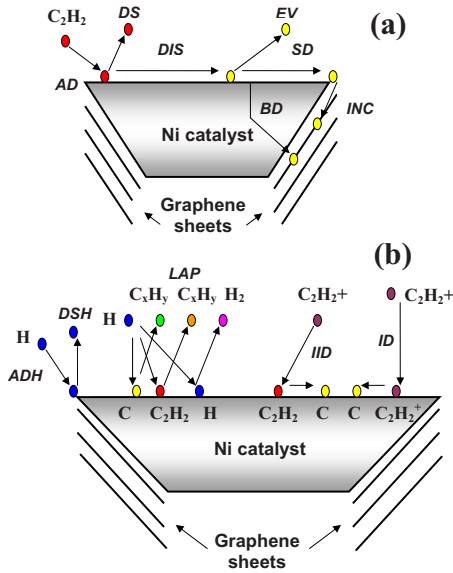
FIG. 1. (Color online) Processes that are common for thermal CVD and PECVD (a) and the additional processes on the catalyst surface that are accounted for in PECVD (b). AD=adsorption of C_2H_2, DS=desorption of C_2H_2 (activation energy E_{aCH}), DIS=dissociation (δE_i), EV=evaporation (E_{ev}), SD=surface diffusion (E_s), INC=incorporation into a graphene sheet (δE_{inc}), BD=bulk diffusion (E_b), ADH=adsorption of H, DSH=desorption of H (activation energy E_{aH}), LAP=loss of adsorbed particles at interaction with atomic hydrogen, IID=ion-induced dissociation of C_2H_2, and ID $=C_2H_2^+$ ion decomposition.

surface of the catalyst nanoparticle is subject to incoming fluxes of hydrocarbon neutrals, etching gas, and hydrocarbon ions (here, C_2H_2, H, and $C_2H_2^+$, respectively). As a result of deposition of the plasma-generated species and a number of elementary processes on the catalyst (see Fig. 1), carbon atoms, the primary building units of the nanofibers, are created on the top surface of the catalyst nanoparticle. It is assumed that the top surface of the catalyst is flat and circular and is covered by C_2H_2, C, and H species with the surface coverages θ_{CH}, θ_C, and θ_H, respectively.

The following processes take place on the catalyst surface:[26,28,33,34] adsorption and desorption of C_2H_2 and H, thermal dissociation of acetylene molecules, evaporation of carbon atoms from the catalyst surface, ion-induced dissociation of C_2H_2, interaction of all the adsorbed species with incoming hydrogen atoms, and dissociation of hydrocarbon ions [Figs. 1(a) and 1(b)]. It is assumed that the carbon atoms incorporate into the growing graphene sheets (shown as stacked cones in Fig. 1) via bulk and surface diffusion.

Using the above mentioned assumptions, the mass balance equations for C, C_2H_2, and H species on the catalyst surface can be written as

$$J_C + \mathrm{div}(D_s\,\mathrm{grad}\,n_C) - O_C = 0, \tag{1}$$

$$Q_{CH} - \theta_{CH} j_i y_d - n_{CH}\nu \exp(-\delta E_i/k_B T_s) = 0, \tag{2}$$

and

$$Q_H + 2n_{CH}\nu \exp(-\delta E_i/k_B T_s) = 0, \tag{3}$$

respectively.

In Eq. (1),

$$J_C = 2n_{CH}\nu \exp(-\delta E_i/k_B T_s) + 2\theta_{CH} j_i y_d + 2j_i$$

is the term that describes the generation of carbon atoms on the catalyst surface due to thermal (with the energy barrier δE_i) and ion-induced dissociation of C_2H_2 and the decomposition of $C_2H_2^+$. The second term in Eq. (1) accounts for the carbon loss due to surface diffusion, whereas

$$O_C = n_C\nu \exp(-E_{ev}/k_B T_s) + n_C\sigma_{ads}j_H$$
$$+ n_C\nu \exp(-E_b/k_B T_s)$$

describes the carbon atom loss due to evaporation (with the energy barrier E_{ev}), interaction of C with atomic hydrogen from the plasma, and C diffusion into the catalyst bulk. Here, $D_s = D_{s0}\exp(-E_s/k_B T_s)$ is the surface diffusion coefficient, where D_{s0} is a constant, k_B is the Boltzmann constant, and E_s is the energy barrier for diffusion of C on the catalyst surface. Likewise, $n_\alpha = \theta_\alpha v_0$ is the surface concentration of species α [subscript α=(CH, H, and C) stands for C_2H_2, H, and C species, respectively], $v_0(\approx 1.3\times 10^{15}$ $cm^{-2})$ is the number of adsorption sites per unit area,[34] and $\nu = 10^{13}$ Hz is the thermal vibrational frequency. Furthermore, $j_i \approx n_i(k_B T_e/m_i)^{1/2}$ is the ion flux, where n_i is the ion density in the plasma, $T_e \approx 1.5$ eV is the electron temperature, and m_i is the ion mass, and $y_d \approx E_i/E_{dis}$, where E_i is the ion energy in eV and $E_{dis}\approx 5.58$ eV is the dissociation energy for a C_2H_2 molecule in a vacuum.[29] Likewise, $\sigma_{ads}(\approx 6.8 \times 10^{-16}$ $cm^2)$ is the cross section for the reactions of atomic hydrogen (with incoming flux j_H) with adsorbed particles[34] and $E_b(\approx 1.6$ eV) is the energy barrier for bulk diffusion.[29]

In Eqs. (2) and (3),

$$Q_\alpha = j_\alpha(1 - \theta_t) - n_\alpha\nu \exp(-E_{a\alpha}/k_B T_s) - n_\alpha\sigma_{ads}j_H,$$

where $E_{a\alpha}$ is the desorption activation energy for species α and $\theta_t = \theta_{CH} + \theta_H + \theta_C$ is the total surface coverage. The first, second, and third terms in the expression for Q_α describe the adsorption, desorption of species α, and interaction of the adsorbed species α with atomic hydrogen from the plasma, respectively. Here, $j_\alpha = \tilde{n}_\alpha v_{th\alpha}/4$ is the flux of the impinging species α and $\tilde{n}_\alpha$ and $v_{th\alpha}$ are the volume density and thermal velocity of species α. The second term in Eq. (2) accounts for C_2H_2 loss due to ion bombardment, whereas the last terms in Eqs. (2) and (3) account for C_2H_2 loss and H generation as a result of thermal dissociation of acetylene.

To find the carbon surface density n_C and other growth parameters from Eqs. (1)–(3), boundary conditions for Eq. (1) are needed. First, we have assumed that the carbon atoms, while diffusing on the catalyst surface, incorporate into the graphene sheets at the border of the catalyst particle ($r = r_p$, where r_p is the catalyst particle radius), with the rate determined from $-D_s dn_C/dr = kn_C$, where $k = A_k\exp(-\delta E_{inc}/k_B T_s)$ is the incorporation speed, A_k is a constant[26] and δE_{inc} is the barrier for C diffusion along the graphene-catalyst interface. Second, it is assumed that at the center of the top surface of the catalyst nanoparticle ($r=0$), the surface diffusion flux vanishes ($\partial n/\partial r|_{r=0} 0$).

Knowing n_C, one can find the diffusion fluxes of carbon atoms to the graphene sheets,

$$J_s = -D_s \frac{dn_C}{dr}\bigg|_{r=r_p} \times 2\pi r_p, \tag{4}$$

$$J_v = \int_0^{r_p} (n_C D_b / r_p^2) 2\pi r dr, \tag{5}$$

over the catalyst particle's surface[28] and through the catalyst bulk, respectively. Here, $D_b = D_{b0}\exp(-E_b/k_B T_s)$ is the bulk diffusion coefficient with D_{b0} as a constant.

The surface and bulk diffusion fluxes determine the surface and bulk diffusion growth rates, $H_s = m_C J_s/(\pi r_p^2 \rho)$ and $H_v = m_C J_v/(\pi r_p^2 \rho)$, respectively. Here, $\rho \approx 2$ g/cm^3 is the CNF material density and m_C is the mass of a carbon atom.

III. SOLUTIONS FOR SURFACE COVERAGES AND FLUX OF CARBON ATOMS

From Eqs. (1)–(3) one can obtain the following equation for the carbon surface density:

$$D_s \frac{1}{r}\frac{d}{dr}\left(r\frac{dn_C}{dr}\right) - n_C/\tau_a + Q_C = 0, \tag{6}$$

where $\tau_a = [C_1/v_0 + \nu \exp(-E_{ev}/k_B T_s) + \sigma_{ads} j_H + \nu \exp(-E_b/k_B T_s)]^{-1}$ is the characteristic residence time of carbon on the catalyst surface, $Q_C = 2j_i + C_1$ is the effective carbon flux to the catalyst surface, $C_1 = [2v_0\nu \exp(-\delta E_i/k_B T_s) + 2j_i y_d]/[1 + Lj_H/(Kj_{CH}) + M/K + L/j_{CH}]$, $L = v_0\nu \exp(-E_{aCH}/k_B T_s) + j_i y_d + v_0\sigma_{ads} j_H + v_0\nu \exp(-\delta E_i/k_B T_s)$, $K = v_0\nu \exp(-E_{aH}/k_B T_s) + v_0\sigma_{ads} j_H$, and $M = 2v_0\nu \exp(-\delta E_i/k_B T_s)$.

Equation (6) has a similar form to the equation describing CNT growth mediated by surface diffusion in CVD.[35,36] The solution of Eq. (6) is

$$n_C(r) = Q_C\tau_a\left(1 - \frac{(k\lambda_D/D_s)I_0(r/\lambda_D)}{I_1(r_p/\lambda_D) + (k\lambda_D/D_s)I_0(r_p/\lambda_D)}\right), \tag{7}$$

where I_0 and I_1 are the modified Bessel functions of the zeroth and first order, respectively, and $\lambda_D = \sqrt{D_s \tau_a}$ is the surface diffusion length. Using Eq. (7), one can find the surface coverages of the catalyst by carbon atoms,

$$\theta_C(r) = n_C(r)/v_0,$$

acetylene molecules,

$$\theta_{CH}(r) = \frac{1 - \theta_C(r)}{1 + Lj_H/(Kj_{CH}) + M/K + L/j_{CH}}, \tag{8}$$

and atomic hydrogen,

$$\theta_H(r) = \theta_{CH}(r)(Lj_H/j_{CH} + M)/K.$$

From Eqs. (4) and (7) it follows that the surface diffusion flux may be expressed as

$$J_s = \frac{2\pi r_p k \tau_a Q_C I_1(r_p/\lambda_D)}{I_1(r_p/\lambda_D) + (k\lambda_D/D_s)I_0(r_p/\lambda_D)}. \tag{9}$$

This expression may be simplified in some limiting cases. For example, at a low rate of carbon atom incorporation into graphene sheets $[I_1(r_p/\lambda_D) \gg (k\lambda_D/D_s)I_0(r_p/\lambda_D)]$, the surface diffusion flux is

$$J_s \approx 2\pi r_p k \tau_a Q_C. \tag{10}$$

At high incorporation rates $[I_1(r_p/\lambda_D) \ll (k\lambda_D/D_s)I_0(r_p/\lambda_D)]$ and small particle radius $[(r_p/\lambda_D) \ll 1]$, the surface diffusion flux becomes

$$J_s \approx \pi r_p^2 Q_C. \tag{11}$$

From Eq. (10) one can see that at low rates of C incorporation the surface diffusion flux depends on the surface diffusion length of carbon on the catalyst surface (since $\tau_a = \lambda_D^2/D_s$), the effective carbon flux, and the speed of incorporation. On the other hand, when the rates of incorporation are high, the surface diffusion flux depends only on the effective carbon flux to the catalyst surface.

In many experiments on CNF growth the particle radius is much smaller than the diffusion length ($r_p/\lambda_D \ll 1$). In this case the ratio of the bulk diffusion flux to that of the surface diffusion flux is

$$J_v/J_s \approx \frac{D_b}{D_s}\left(\frac{D_s}{2kr_p} + \frac{1}{8}\right). \tag{12}$$

From Eq. (12) it follows that if the energy barrier of bulk diffusion is larger than that of surface diffusion and diffusion along the graphene-catalyst interface ($E_b > E_s, \delta E_{inc}$), then the ratio J_v/J_s becomes larger with an increase in T_s. Therefore, at relatively large surface temperatures the effect of bulk diffusion on the CNF growth may be significant. Thus, at low T_s, one can expect that the effect of the surface diffusion is more important than that of the bulk diffusion in PECVD. These conclusions are in good agreement with the results of previous studies.[28]

Under conditions of intense ion bombardment the surface coverage by hydrogen atoms may be small.[37] In this case, $\theta_t \approx \theta_C + \theta_{CH}$, and the carbon surface density is described by Eq. (6) with $C_1 \approx [2v_0\nu \exp(-\delta E_i/k_B T_s) + 2j_i y_d]/(1 + L/j_{CH})$. For the $\theta_H \approx 0$ case, the surface coverage of the catalyst by hydrocarbon molecules is $\theta_{CH} \approx j_{CH}(1 - \theta_C)/(L + j_{CH})$.

IV. DEPENDENCE OF GROWTH PARAMETERS ON SURFACE TEMPERATURE AND ION AND ETCHING GAS DENSITIES

Using the analytical results presented in Sec. III, we will now study and examine how the parameters that characterize CNF growth (the nanostructure growth rates, the effective carbon flux to the catalyst surface, the characteristic residence time and diffusion length of carbon adatoms on the catalyst surface, and the surface coverages) depend on the catalyst surface temperature, etching gas, and ion densities. To find such dependencies, we varied the surface temperature, as well as the etching gas and ion densities in our calculations, and then observed how these changes affected the nanofiber growth parameters.

In Fig. 2(a), the dependencies of H_v, H_s, and H_t ($=H_s + H_v$) on the surface temperature are shown. The curves have been plotted assuming that hydrogen atoms are present on the catalyst surface. One can see in this figure that the surface diffusion curve is the best fit for the experimental data of Hofmann *et al.*[21,29] in the broad range of temperatures considered.
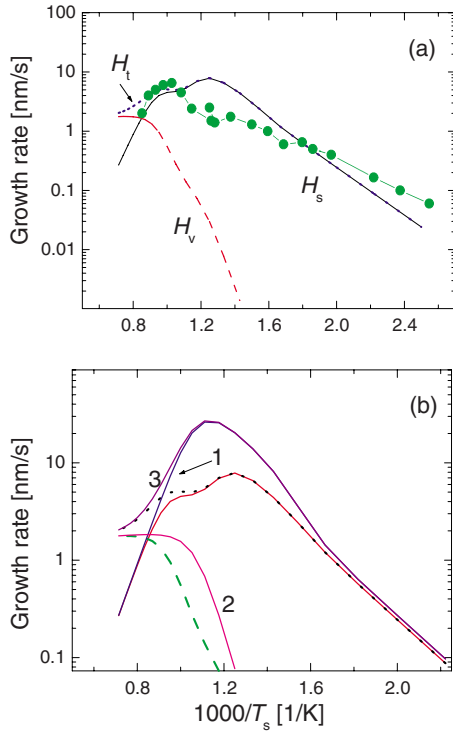
FIG. 2. (Color online) (a) H_s, H_v, and H_t in PECVD as functions of the substrate temperature for $\theta_H \neq 0$, $\tilde{n}_{CH} = 7 \times 10^{14}$ cm^{-3}, $\tilde{n}_H = 3 \times 10^{-2} \tilde{n}_{CH}$, $E_i = 500$ eV, $n_i = 3 \times 10^{10}$ cm^{-3}, $r_p = 25$ nm, $E_{aCH} = 2.9$ eV, $E_{aH} = E_{ev} = 1.8$ eV, $\delta E_i = 1.3$ eV, $E_s = 0.3$ eV, and $\delta E_{inc} = 0.4$ eV (a). The circles correspond to experimental data taken from Ref. 21. (b) H_s (curve 1 and unnumbered solid curve), H_v (curve 2 and dashed curve), and H_t (curve 3 and dotted curve) for $\theta_H = 0$ and $\theta_H \neq 0$, respectively. All other parameters are the same as in (a).
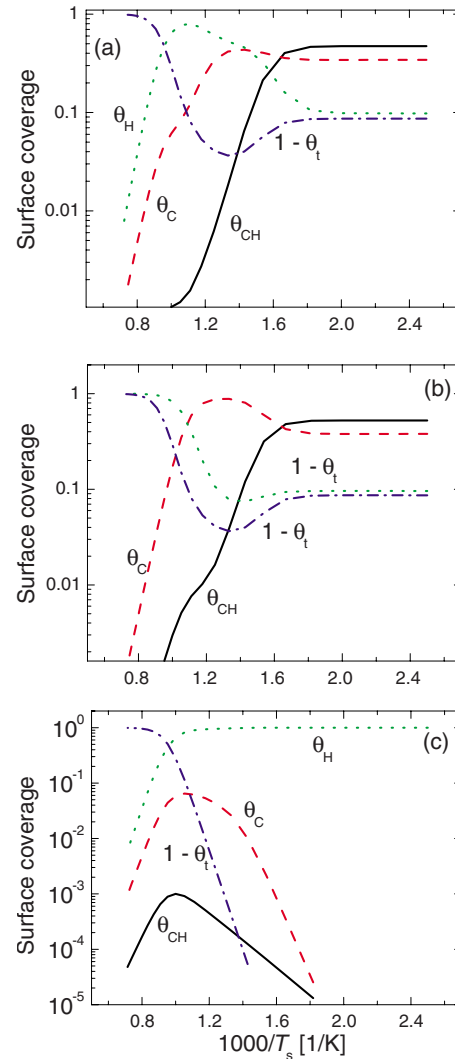

FIG. 3. (Color online) The surface coverages in the $\theta_H \neq 0$ (a), $\theta_H = 0$ (b), and $j_i = 0$, $j_H = 0$ (c) cases. The dashed-dotted curve in (b) corresponds to $1 - \theta_t$ for the $\theta_H \neq 0$ case. The external conditions are the same as in Fig. 2(a).

In Fig. 2(b), the growth rates H_t, H_v, and H_s, obtained under the assumption $\theta_H \neq 0$, are compared with those calculated for the extreme case when the surface coverage by atomic hydrogen is negligibly small ($\theta_H = 0$). Since the area of the uncovered catalyst surface at $\theta_H = 0$ is larger than that at $\theta_H \neq 0$ [Fig. 3(b)], the effective carbon flux Q_C (Fig. 4) and hence the growth rates [Fig. 2(b)] at $\theta_H = 0$ in the temperature range $0.9 < \beta_T = 1000 / T_s < 1.8$ are larger than the corresponding parameters calculated at $\theta_H \neq 0$.

In the plasma-assisted process (at $\theta_H = 0$ as well as $\theta_H \neq 0$), the surface coverage of the catalyst by carbon atoms at low T_s is large compared to θ_C at higher surface temperatures [Figs. 3(a) and 3(b)]. The increase in θ_C at small T_s is due to a reduction in evaporation and desorption of C and C_2H_2 species. At low T_s, the loss and generation of carbon atoms on the catalyst surface are governed mainly by the interaction of particles on the catalyst with incoming ions and etching gas fluxes from the plasma.[28] It is noteworthy that under the conditions considered here ($j_H \ll j_{CH}$), even assuming $\theta_H \neq 0$, the catalyst coverage by hydrogen in PECVD is relatively small at low surface temperatures [Fig. 3(a)].

For comparison, let us now consider the surface coverage in thermal CVD ($j_i = 0$, $j_H = 0$). At low T_s, the surface coverage of the catalyst by carbon atoms in the CVD process is quite low [Fig. 3(c)]. The main reason is less effective production of carbon atoms via thermal dissociation of C_2H_2. For the case considered here the barrier of thermal dissociation of acetylene is smaller than the barrier for the atomic

hydrogen desorption; thus the hydrogen coverage in CVD is large at low T_s [Fig. 3(c)]. In PECVD, carbon atoms on the catalyst are generated not only through thermal dissociation but also via ion-induced processes. As a result, at low T_s the effective carbon flux and the surface coverage of the catalyst
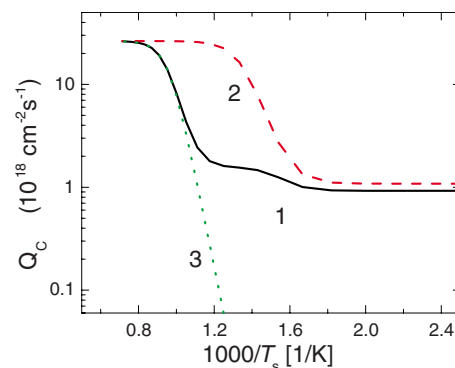

FIG. 4. (Color online) The effective carbon flux for the $\theta_H \neq 0$ (curve 1), $\theta_H = 0$ (curve 2), and $j_i = 0$, $j_H = 0$ (curve 3) cases. The external conditions are the same as in Fig. 2(a).
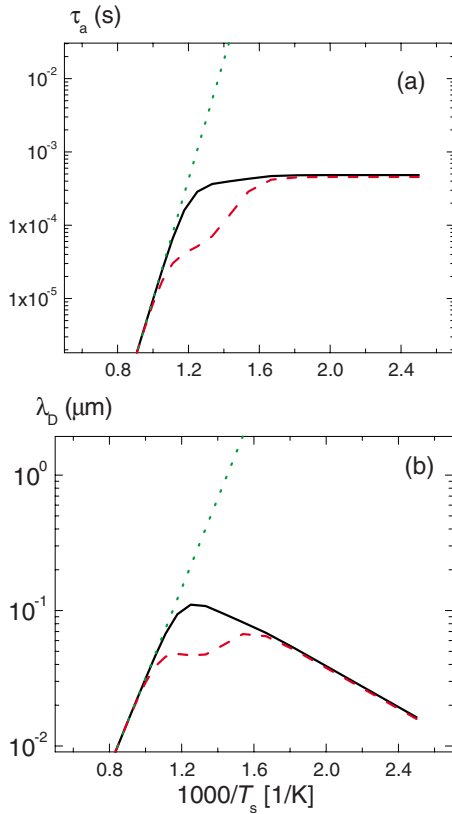
FIG. 5. (Color online) The residence time (a) and diffusion length (b) for the $\theta_H \neq 0$ (solid curve), $\theta_H = 0$ (dashed curve), and $j_i = 0, j_H = 0$ (dotted curve) cases. The external conditions are the same as in Fig. 2(a).

FIG. 6. (Color online) The growth rate (a), effective carbon flux (b), and residence time (c) for $n_i = 5 \times 10^{11}$ (solid curve), 5×10^{10} (dashed curve), 5×10^9 (dotted curve), and 0 (dashed-dotted curve) cm^{-3}. The curves are obtained for $\theta_H \neq 0$ and for the other external parameters, same as in Fig. 2(a).

surface by carbon atoms in PECVD are much larger than the corresponding parameters in CVD (Figs. 3 and 4).

We have also calculated the carbon residence time and surface diffusion length in the CVD and PECVD cases. Figures 5(a) and 5(b) show the dependencies of τ_a and λ_D on β_T, respectively. One can notice that at relatively high surface temperatures ($\beta_T \leq 1.0$) the residence time and the effective diffusion length, calculated assuming $\theta_H \neq 0$, are approximately the same as the corresponding parameters at $\theta_H = 0$ or in CVD ($j_i = 0$, $j_H = 0$). However, for the temperature range $1.0 \leq \beta_T \leq 1.8$, the residence time and diffusion length at $\theta_H \neq 0$ are larger than those obtained in the $\theta_H = 0$ case. This difference can be explained by the difference in the effective flux Q_C and the value C_1 in the two cases (see Fig. 4). Since at small T_s the effective carbon flux in PECVD (at $\theta_H = 0$ or $\theta_H \neq 0$) is very different from Q_C in CVD, the adatom residence time and the associated diffusion length also appear to be quite different in CVD and PECVD.

Let us now turn our attention to the effects of the ion flux variation. In Fig. 6(a), the dependencies of the growth rate H_t on the surface temperature T_s are shown for different ion densities n_i. One can see from Fig. 6(a) that the ions affect the CNF growth mainly at relatively low temperatures ($\beta_T > 1.2$) and that the rate of growth in the low-temperature range increases for higher ion densities. This increase is due to a stronger effective carbon flux to the catalyst surface Q_C [Fig. 6(b)]. The flux increases because of the enhanced generation of carbon atoms in ion-induced processes.[28] However, the growth rate changes with n_i nonlinearly as can be
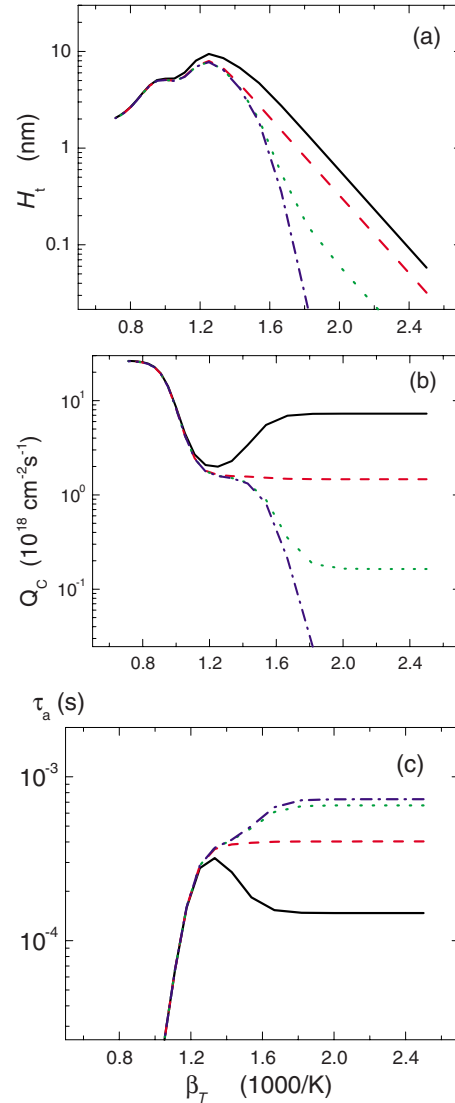
seen in Fig. 6(a). Since at low T_s and large n_i the surface coverage by carbon adatoms is almost complete [Fig. 7(d)], the number of sites for the generation of carbon atoms in ion-induced processes is very limited. In this case, any further increase in n_i may only slightly increase H_t [see dashed and solid curves in Fig. 6(a)]. Moreover, at extremely large j_i the CNF growth may stop due to the overpopulation of the catalyst surface by carbon atoms. This can be regarded as a surface equivalent of the commonly known process of catalyst poisoning.[38] Since the magnitudes of Q_C and C_1 increase with an increase in n_i at a low catalyst temperature, the species residence time decreases when the ion density becomes higher [Fig. 6(c)].

The ion flux also affects the surface coverages θ_C, θ_{CH}, and θ_H. In Fig. 7(a)–7(d) the surface coverages as functions of T_s are shown for $n_i = 0$, 5×10^9, 5×10^{10}, and 5×10^{11} cm^{-3}, respectively. One can see from the figures that at low T_s, the surface coverage by C$_2$H$_2$ decreases and the
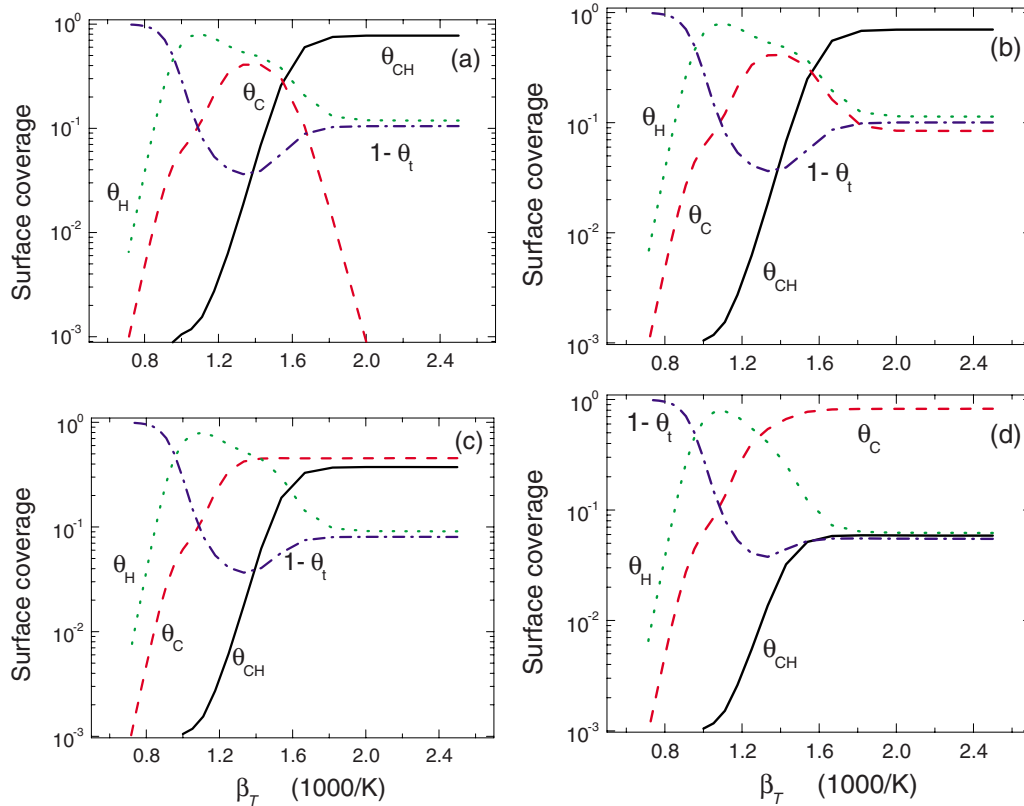
FIG. 7. (Color online) The surface coverage by C_2H_2 (solid curve), C (dashed curve), and by atomic hydrogen (dotted curve), and $1 - \theta_t$ (dashed-dotted curve) for $n_i = 0$ (a), 5×10^9 (b), 5×10^{10} (c), and 5×10^{11} (d) cm^{-3}. The other external parameters are the same as in Fig. 6.

coverage by carbon atoms increases with an increase in n_i. These changes in the C_2H_2 and C coverages at low T_s are due to ion-induced dissociation of C_2H_2 molecules and $C_2H_2^+$ ion decomposition on the catalyst surface. The ion flux also affects the surface coverage θ_H and the value $1 - \theta_t$ which is a characteristic of the area uncovered by adsorbed species. Since the surface coverages θ_{CH} or θ_C are large at low T_s, the other quantities θ_H and $1 - \theta_t$ turn out to be small.

The growth parameters also depend on the hydrogen atom deposition. At low T_s ($\beta_T \gtrsim 1.6$), the surface diffusion and total growth rates, as well as the residence time τ_a, decrease with an increase in $\tilde{n}_H$ due to the interaction of carbon and hydrocarbon particles on the catalyst surface with incoming hydrogen flux [see Figs. 8(a) and 8(b) and Ref. 28]. In the temperature range $1.0 < \beta_T < 1.6$, an enhancement of the etching gas deposition may be accompanied by the CNF growth rate increase due to enhancement of C_2H_2 deposition which is caused by an increase in the value $1 - \theta_t$ [Figs. 9(a)–9(d)].

The incoming hydrogen flux significantly affects the surface coverages of the catalyst surface [Figs. 9(a)–9(d)]. The surface coverage by carbon atoms decreases while the areas covered by the hydrogen atoms increase at larger j_H. When j_H increases, the hydrogen atoms become the main species that are effectively adsorbed on the catalyst surface.

V. DISCUSSION

In this section we will discuss the results obtained, limitations of the CNF growth model, and some issues related to the growth of CNFs in plasma-assisted processes. We have
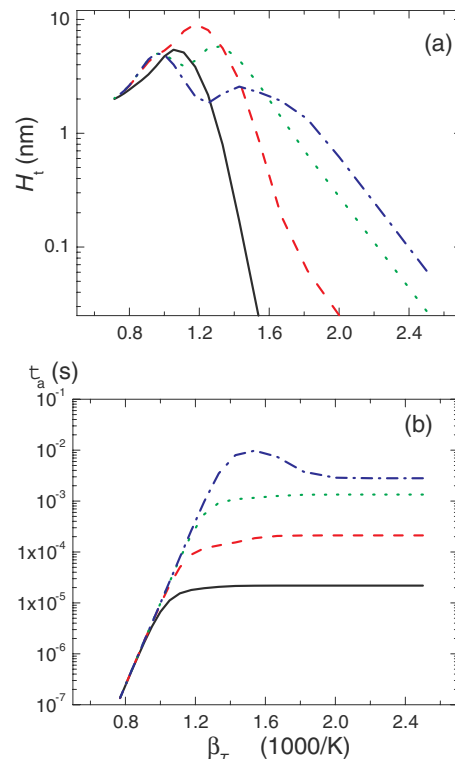

FIG. 8. (Color online) The growth rate (a) and residence time (b) for $\tilde{n}_H = \tilde{n}_{CH}$ (solid curve), $\tilde{n}_H = 0.1 \tilde{n}_{CH}$ (dashed curve), $\tilde{n}_H = 0.01 \tilde{n}_{CH}$ (dotted curve), and $\tilde{n}_H = 10^{-3} \times \tilde{n}_{CH}$ (dashed-dotted curve). Here, $n_i = 10^{10}$ cm^{-3} and the other external parameters are the same as in Fig. 7.
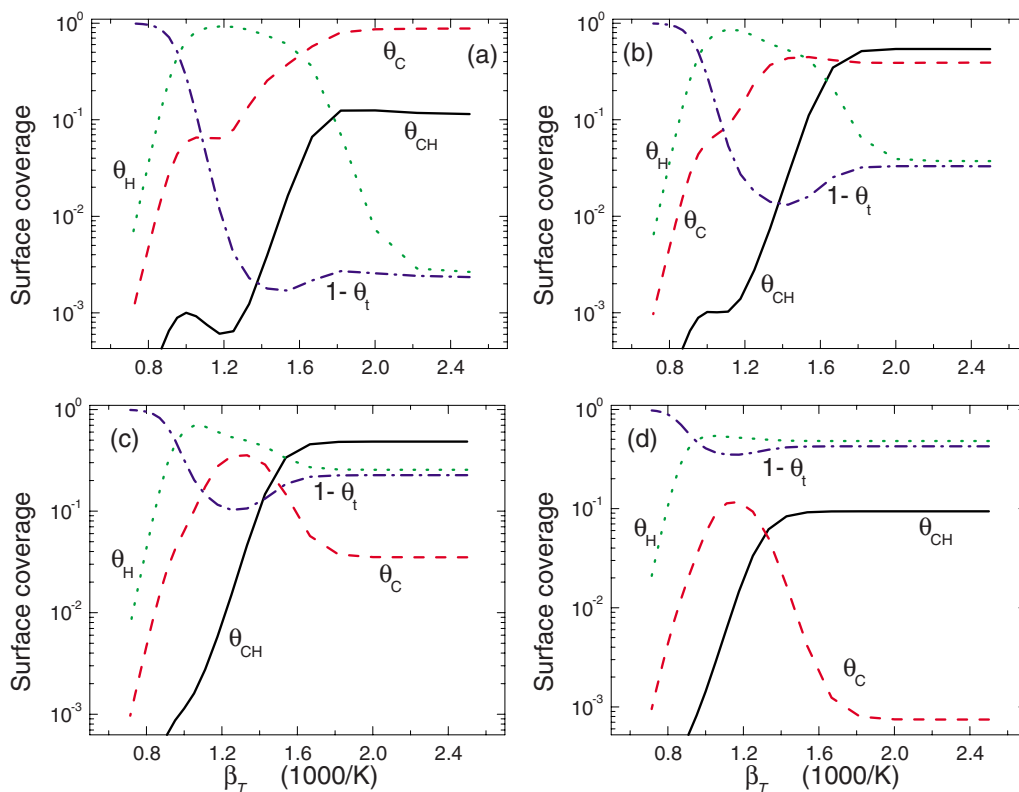
FIG. 9. (Color online) The surface coverage by C_2H_2 (solid curve), C (dashed curve), and by atomic hydrogen (dotted curve), and $1 - \theta_t$ (dashed-dotted curve) for $\tilde{n}_H = 10^{-3} \times \tilde{n}_{CH}$ (a), $\tilde{n}_H = 0.01\tilde{n}_{CH}$ (b), $\tilde{n}_H = 0.1\tilde{n}_{CH}$ (c), and $\tilde{n}_H = \tilde{n}_{CH}$ (d). The other external parameters are the same as in Fig. 8.

shown that at low substrate temperatures the effects of the plasma environment on the CNF growth parameters (the surface diffusion growth rate, the effective carbon flux to the catalyst surface, the characteristic residence time and diffusion length of carbon adatoms on the catalyst surface, and the associated surface coverages) are pronounced. In particular, the ions from the plasma that bombard the catalyst surface may induce dissociation of hydrocarbon neutrals adsorbed on the catalyst nanoparticle. Moreover, hydrocarbon ions while being decomposed on the catalyst surface provide an additional supply of carbon material for CNF growth in the plasma-assisted processes. As a result of ion bombardment, the surface coverage of the catalyst by carbon atoms increases (Fig. 7), providing much higher growth rates in PECVD compared with the growth rates in CVD. Our results are consistent with the experimental results on CNF/CNT growth of Tanemura *et al.*[31] and Woo *et al.*,[32] which show that the nanofibers do not grow when an ion-repelling positive potential is applied to the substrate, as well as when the ion-attracting negative potential of the substrate surface is small.

However, in order to provide conditions for the effective deposition of carbon nanostructures one has to control the ion flux to the substrate. At high ion flux densities, the number of ion-produced carbon adatoms on the catalyst surface may be larger than the number of adsorbed sites on the catalyst. As a result of this obvious oversupply of carbon material, a carbon nanostructure may emerge on the top of the catalyst particle, preventing the plasma-assisted growth of CNFs with a metal catalyst particle on top. The ions from the plasma may also facilitate radical and ion production near

the substrate.[39] The neutral and ion fluxes from the plasma heat the catalyst particle on top of a CNF, increasing its temperature with respect to the substrate temperature.[40] It was shown recently that ion heating effect is also very important for the formation of other nanostructures, in particular, nanodots.[41] The ions may also play an important role in the formation of other high-aspect-ratio nanostructures, such as nanotips and nanocones.[42–45]

However, one should use plasma-based processes with a certain degree of caution. Indeed, there is a larger (as compared to thermal CVD processes) variety of species that are deposited from the plasma onto the catalyst nanoparticle. This may eventually lead to substantial catalyst poisoning. To prevent the undesired overpopulation (and eventually blockage) of the catalyst surface, one has to remove the undesired particles, for example, using reactive chemical etching. However, the flux of the etching gas on the catalyst also has to be moderate. At large etching gas fluxes, the growth rates, residence time, and carbon coverage may become very small, as suggested by the results in Figs. 8 and 9, and thus insufficient for effective CNF growth. The experiments of Okita *et al.*[9] have shown that excessive supply of the etching gas makes the diameter distribution of vertically aligned carbon nanostructures broader and also reduces the process yield.

It is notable that our model has some limitations. First, we have only studied here the so-called CNF growth period with a high growth rate. In addition to this growth stage, there is also the incubation period prior to the start of rapid CNF growth and yet another stage when the CNF growth is slowed down and eventually saturated. All the growth stages

depend on the experimental conditions, in particular, on the ratio of C and H densities in the plasma.[46,47] Second, from our modeling results it still remains unclear exactly how the atomic hydrogen behaves on the catalyst surface and inside the catalyst nanoparticle. The growth rates calculated under assumptions $\theta_H \neq 0$ and $\theta_H = 0$ are in good qualitative agreement with the available experimental data (Fig. 2). Our model does not account for the nanofiber heating by the plasma fluxes nor have we considered any processes of carbon nucleation into graphite on the catalyst nanoparticle surface which is possible at large surface coverages by carbon [Figs. 7(d) and 9(a)]. Migration of hydrogen atoms and their interaction with other adsorbed species on the surface have also been neglected. Neglect of these important effects may lead to overestimation of the surface coverages. Moreover, in our model the flux densities of C_2H_2, $C_2H_2^+$, and H are input parameters. In reality, the neutral and ion fluxes depend on neutral gas composition and pressure, input power,9+ and substrate bias. Consequently, the number of species deposited on the catalyst particle in the plasma-assisted process may be much larger than what was predicted in this work. To obtain a better insight into PECVD of CNFs and related nanostructures, the model should be complemented by the appropriate chemistry and gas discharge models.

VI. CONCLUSIONS

Thus, we have presented a model describing the plasma-assisted growth of CNFs. Using the model, we have studied the plasma-related effects on the CNF growth parameters such as the growth rate due to surface and bulk diffusion, the effective carbon flux onto the catalyst surface, the characteristic residence time, the diffusion length of carbon adatoms on the catalyst surface, as well as the associated surface coverages. It has also been demonstrated how these parameters depend on the catalyst surface temperature and ion and etching gas fluxes onto the catalyst. Specific conditions under which a low-temperature plasma environment can benefit the CNF growth have been formulated.

The main conclusions based on the results obtained in this work can be summarized as follows.

- Ion-induced dissociation of hydrocarbon molecules and radicals, adsorption, and decomposition of hydrocarbon ions on the catalyst surface are essential sources of carbon atoms required for the CNF growth. Due to ion bombardment, the carbon atoms are the main species that cover the catalyst nanoparticles at low substrate temperatures. It is in contrast with the thermal CVD case, where the catalyst surface at low T_s is covered mainly by hydrogen atoms.
- The impinging hydrogen atoms can prevent oversupply of carbon material to the catalyst particles and can condition the catalyst against unwanted adsorbates.
- The characteristic residence time and the diffusion length of carbon adatoms on the catalyst nanoparticle surface decrease when the ion and/or etching gas densities become higher.
- A suitable control of the ion and etching gas fluxes onto the catalyst nanoparticles can enable rapid growth

of very-high-aspect-ratio CNFs at surface temperatures substantially lower than those in thermal CVD.
- However, at low substrate temperatures, one should minimize several adverse effects by carefully balancing the incoming fluxes of the plasma ions and etching gas. If the ion flux is too high and the etching process is not strong enough, excessive production of carbon adatoms and/or other adsorbents can block the access of carbon adatoms to the graphene sheets. This can eventually terminate the CNF growth.
- We note that the effects of the plasma environment on the CNF growth are particularly important for $T_s \leq 1000$ K. At higher substrate temperatures the role of thermal processes in carbon atom supply for PECVD is clearly dominant over the ion-induced processes.

Moreover, the CNFs may be postprocessed in the same discharge chambers where they were deposited. By controlling plasma-extracted ion fluxes and varying the plasma and sheath parameters, one can selectively coat, dope, or functionalize different areas on nanofiber/nanotube surfaces.[48,49] The model and numerical results presented here can be used for optimizing CNF and nanotube synthesis and for analyzing processes in PECVD. The main conclusions obtained here are not restricted to carbon nonofibers and nanotubes and can also be relevant to the plasma-assisted growth of a broader range of nanostructures.

ACKNOWLEDGMENTS

[1]M. Meyyappan, L. Delzeit, A. Cassell, and D. Hash, Plasma Sources Sci. Technol. **12**, 205 (2003).
[2]A. V. Melechko, V. I. Merkulov, T. E. McKnight, M. A. Guillorn, K. L. Klein, D. H. Lowndes, and M. L. Simpson, J. Appl. Phys. **97**, 041301 (2005).
[3]M. Mozetic, U. Cvelbar, M. K. Sunkara, and S. Vaddiraju, Adv. Mater. (Weinheim, Ger.) **17**, 2138 (2005).
[4]U. Cvelbar and M. Mozetic, J. Phys. D **40**, 2300 (2007).
[5]M. Keidar, Y. Raitses, A. Knapp, and A. M. Waas, Carbon **44**, 1022 (2006).
[6]E. I. Waldorff, A. M. Waas, P. P. Friedmann, and M. Keidar, J. Appl. Phys. **95**, 2749 (2004).
[7]M. Xu, S. Xu, J. W. Chai, J. D. Long, and Y. C. Ee, Appl. Phys. Lett. **89**, 251904 (2006).
[8]A. Okita, Y. Suda, A. Ozeki, H. Sugawara, Y. Sakai, A. Oda, and J. Nakamura, J. Appl. Phys. **99**, 014302 (2006).
[9]K. N. Ostrikov, M. Y. Yu, and H. Sugai, J. Appl. Phys. **86**, 2425 (1999).
[10]K. Ostrikov and A. B. Murphy, J. Phys. D **40**, 2223 (2007).
[11]S. Sharma and M. K. Sunkara, Nanotechnology **15**, 130 (2004); J. Am. Chem. Soc. **124**, 12288 (2002).
[12]V. Nemanic, M. Zumer, B. Zajec, D. Mihailovich, D. Vengust, and B. Podobnik, J. Appl. Phys. **103**, 094310 (2008).
[13]J. Robertson, Mater. Today **10**, 36 (2007).
[14]K. Ostrikov, Rev. Mod. Phys. **77**, 489 (2005).
[15]F. J. Gordillo-Vazquez, V. J. Herrero, and I. Tanarro, Chem. Vap. Deposition **13**, 267 (2007).
[16]S. Xu, K. N. Ostrikov, Y. Li, E. L. Tsakadze, and I. R. Jones, Phys.

Plasmas **8**, 2549 (2001); K. N. Ostrikov, M. Y. Yu, S. V. Vladimirov, and O. Ishihara, Phys. Plasmas **6**, 737 (1999).

[17]N. A. Azarenkov, I. B. Denisenko, and K. N. Ostrikov, J. Phys. D **28**, 2465 (1995); S. V. Vladimirov, K. N. Ostrikov, M. Y. Yu, and L. Stenflo, Phys. Rev. E **58**, 8046 (1998).

[18]K. Ostrikov, I. B. Denysenko, S. V. Vladimirov, S. Xu, H. Sugai, and M. Y. Yu, Phys. Rev. E **67**, 056408 (2003); K. N. Ostrikov, M. Y. Yu, and L. Stenflo, Phys. Rev. E **61**, 782 (2000).

[19]M. Keidar, I. Levchenko, T. Arbel, M. Alexander, A. M. Waas, and K. Ostrikov, Appl. Phys. Lett. **92**, 043129 (2008).

[20]S. Y. Xu, J. D. Long, L. N. Smith, C. H. Diong, and K. Ostrikov, Plasma Processes Polym. **2**, 373 (2005).

[21]S. Hofmann, C. Ducati, J. Robertson, and B. Kleinsorge, Appl. Phys. Lett. **83**, 135 (2003).

[22]I. B. Denysenko, S. Xu, J. D. Long, P. P. Rutkevych, N. A. Azarenkov, and K. Ostrikov, J. Appl. Phys. **95**, 2713 (2004).

[23]D. B. Hash, M. S. Bell, K. B. K. Teo, B. A. Cruden, W. I. Milne, and M. Meyyappan, Nanotechnology **16**, 925 (2005).

[24]L. Zajickova, M. Elias, O. Jasek, V. Kudrle, Z. Frgala, J. Matejkova, J. Bursik, and M. Kadlecikova, Plasma Phys. Controlled Fusion **47**, B655 (2005).

[25]F. J. Gordillo-Vazquez and J. M. Albella, Plasma Sources Sci. Technol. **13**, 50 (2004).

[26]O. A. Louchev, T. Laude, Y. Sato, and H. Kanda, J. Chem. Phys. **118**, 7622 (2003).

[27]C. Klinke, J. M. Bonard, and K. Kern, Phys. Rev. B **71**, 035403 (2005).

[28]I. Denysenko and K. Ostrikov, Appl. Phys. Lett. **90**, 251501 (2007).

[29]S. Hofmann, G. Czanyi, A. C. Ferrari, M. C. Payne, and J. Robertson, Phys. Rev. Lett. **95**, 036101 (2005), and the references therein.

[30]I. Denysenko, K. Ostrikov, M. Y. Yu, and N. A. Azarenkov, J. Appl. Phys. **102**, 074308 (2007).

[31]M. Tanemura, K. Iwata, K. Takahashi, Y. Fujimoto, F. Okuyama, H. Sugie, and V. Filip, J. Appl. Phys. **90**, 1529 (2001).

[32]Y. S. Woo, I. T. Han, Y. J. Park, H. J. Kim, J. E. Jung, N. S. Lee, D. Y. Jeon, and J. M. Kim, Jpn. J. Appl. Phys., Part 1 **42**, 1410 (2003).

[33]O. A. Louchev, C. Dussarrat, and Y. Sato, J. Appl. Phys. **86**, 1736 (1999).

[34]N. V. Mantzaris, E. Gogolides, A. G. Boudouvis, A. Rhallabi, and G. Turban, J. Appl. Phys. **79**, 3718 (1996).

[35]O. A. Louchev, Phys. Status Solidi A **193**, 585 (2002).

[36]O. A. Louchev, J. Cryst. Growth **237–239**, 65 (2002).

[37]C. Hopf, A. von Keudell, and W. Jacob, J. Appl. Phys. **93**, 3352 (2003).

[38]I. Levchenko and K. Ostrikov, Appl. Phys. Lett. **92**, 063108 (2008).

[39]M. Chhowalla, K. B. K. Teo, C. Ducati, N. L. Rupesinghe, G. A. J. Amaratunga, A. C. Ferrari, D. Roy, J. Robertson, and W. I. Milne, J. Appl. Phys. **90**, 5308 (2001).

[40]K. B. K. Teo, D. B. Hash, R. G. Lacerda, N. L. Rupesinghe, M. S. Bell, S. H. Dalal, D. Bose, T. R. Govindan, B. A. Cruden, M. Chhowalla, G. A. J. Amaratunga, M. Meyyappan, and W. I. Milne, Nano Lett. **4**, 921 (2004).

[41]A. E. Rider, K. Ostrikov, and I. Levchenko, Nanotechnology **19**, 355705 (2008).

[42]B. Wang and B. Zhang, Diamond Relat. Mater. **16**, 1982 (2007).

[43]K. Ostrikov, Z. Tsakadze, P. P. Rutkevych, J. D. Long, S. Xu, and I. Denysenko, Contrib. Plasma Phys. **45**, 514 (2005).

[44]K. Ostrikov, J. D. Long, P. P. Rutkevych, and S. Xu, Vacuum **80**, 1126 (2006).

[45]E. Tam, I. Levchenko, and K. Ostrikov, J. Appl. Phys. **100**, 036104 (2006).

[46]G. Zhang, D. Mann, L. Zhang, A. Javey, Y. Li, E. Yenilmez, Q. Wang, J. P. McVittie, Y. Nishi, J. Gibbons, and H. Dai, Proc. Natl. Acad. Sci. U.S.A. **102**, 16141 (2005).

[47]M. R. Maschmann, P. B. Amama, A. Goyal, Z. Iqbal, R. Gat, and T. S. Fisher, Carbon **44**, 10 (2006).

[48]I. Levchenko, K. Ostrikov, and E. Tam, Appl. Phys. Lett. **89**, 223108 (2006).

[49]I. Levchenko, K. Ostrikov, M. Keidar, and S. Xu, J. Appl. Phys. **98**, 064304 (2005).